Accepted Manuscript

An idealised study for the evolution of a shoreface nourishment

W.L. Chen, N. Dodd

PII: S0278-4343(19)30052-4

DOI: https://doi.org/10.1016/j.csr.2019.03.010

Reference: CSR 3894

To appear in: *Continental Shelf Research*

Received Date: 15 January 2019

Revised Date: 20 March 2019

Accepted Date: 27 March 2019

Please cite this article as: Chen, W.L., Dodd, N., An idealised study for the evolution of a shoreface nourishment, *Continental Shelf Research* (2019), doi: https://doi.org/10.1016/j.csr.2019.03.010.

An idealised study for the evolution of a shoreface nourishment

W.L. Chen, [a,*] N. Dodd [a]

[a] *Faculty of Engineering, University of Nottingham, Nottingham NG7 2RD, UK.*

Abstract

We develop an idealised one dimensional (cross-shore) morphodynamic model that couples wave, tide and sediment dynamics to study the effect and evolution of a shoreface nourishment. Sediment fluxes driven by wave skewness, wave asymmetry (both onshore) and return flow (offshore) are considered. With the aid of new analytical expressions for the skewness and standard deviation of wave velocity and acceleration, sediment fluxes are calculated. Nourishment is viewed as a perturbation to the system in equilibrium that is subject to the divergence of the perturbed sediment flux and a gravity driven diffusion term. Depending on the location, a nourishment may provide a feeder or lee effect. In moderate and mild wave conditions, the evolution of a nourishment primarily depends on the relative location of nourishment and break point. Placed well offshore of the break point, the nourishment induces an overall positive perturbation in sediment flux, resulting in onshore migration (feeder effect). Located closer to the break point, the nourishment induces an earlier wave breaking, which dissipates part of the wave energy (lee effect), leading to a negative sediment flux perturbation around this break point and a positive sediment flux perturbation around the break point of the un-nourished beach. Depending on the intensity of the earlier breaking, the nourishment either migrates onshore (weak break) or splits into onshore and offshore moving parts (strong break). The relative importance of the diffusion term and the divergence of perturbed sediment flux may lead to a primarily migrating or decaying evolution of nourishment. In storm wave conditions, the nourishment tends to move offshore due to the predominance of return flow driven sediment flux. The sensitivity to wave period and tide are also studied. Model results are consistent with observations, as well as prevailing theory on cross-shore sediment transport.

Key words: Shoreface nourishment, wave skewness, wave asymmetry, return flow, lee effect, feeder effect

* Corresponding author, wenlong.chen@nottingham.ac.uk

1 Introduction

A nourishment placed in the shoreface region is considered as an effective treatment against a shore erosion problem (*Capobianco et al.*, 2002). Based on the so called 'lee' effect (*Ojeda et al.*, 2008), which refers to the ability of nourishment to increase wave dissipation, a shoreface nourishment is expected to reduce the wave energy approaching the shore, thus providing protection. Moreover, the nourishment serves as a source for the onshore movement of sediment, which is often described as the 'feeder' effect (*van Duin et al.*, 2004). Compared with traditional technologies, e.g., offshore breakwater, such 'soft' engineering is considered more environmentally friendly and incurs less cost (*Hamm et al.*, 2002). A thorough understanding of the subsequent evolution of a nourishment can aid design of the nourishment project so as to achieve the maximum effect. Therefore, it is important to understand the underlying physics involved in the nourishment evolution.

A common way to study the evolution of a nourishment is using complex numerical models which couple wave, tide and sediment dynamics (*van Duin et al.*, 2004; *Roelvink and Reniers*, 2011; *Samaras et al.*, 2016). The placement of the nourishment changes the topography and thus affects the hydrodynamics which in turn drives the evolution of the nourishment. This method aims at accurate simulation of the actual topography, and thus is useful for practical purposes. However, the evolution of the nourishment is embedded in the evolution of the whole coastal area, which makes it difficult to isolate the role of various physics in the evolution of the nourishment alone. Furthermore, running a complex numerical model is very time consuming, and can thus limit the use of such models.

Alternatively, *van Leeuwen et al.* (2007) in an approach also used by *van Veelen et al.* (2018) considered a shoreface nourishment as a perturbation. The linear evolution of a nourishment is then studied using a linear stability model. A longer nourishment (in a longshore sense) is found to decay more slowly than a short one, and shows a shoreward movement during its decay. However, only decaying behavior of the nourishment is considered. *Larson and Hanson* (2015) also considered a nourishment as a perturbation on a sea bed initially in equilibrium, in which the onshore sediment transport, driven by wave asymmetry, and down-slope transport driven by gravity are in balance. The introduction of the nourishment is assumed to perturb the down-slope transport only. *Larson and Hanson* (2015) then use a diffusion equation to describe the response of the nourishment. The model provides the information on how quickly a nourishment disperses, but the on- or off-shore movement of the nourishment is not captured.

The placement of a nourishment also changes other on- and off-shore sediment processes, such as the sediment flux driven by wave skewness, wave asymmetry, and the return flow. As a wave shoals, the wave shape changes from sinusoidal to an increasingly skewed shape, with a narrow accentuated crest followed by a broad flat trough. Assuming no phase shift as the free stream wave velocity is translated into a near bed velocity, the sediment flux, which is proportional to the cubic or higher order of near bed velocity under this wave shape, then shows a net onshore value in a wave averaged sense (*Roelvink and Reniers*, 2011). After breaking, the wave shape progressively changes to a highly asymmetrical shape, i.e., a pitched-forward shape with a steep front face (*Hoefel and Elgar*, 2003). *Henderson et al.* (2004) suggested that the phase shift between near bed velocity and free stream velocity depends on the free-stream asymmetry. Under asymmetrical waves, the phase shift introduces skewness in the near bed velocity and hence leads to an onshore wave averaged sediment flux. *Hoefel and Elgar* (2003) used free stream velocity acceleration as a proxy for this onshore sediment flux. Such a mechanism is critical in explaining the onshore migration of a sandbar, as further identified by *Fernández-Mora et al.* (2015). Additionally, near bed return flow occurs to compensate for the onshore mass flux driven by wave drift and surface roller in the surf zone (*Kuriyama and Nakatsukasa*, 2000). Thus the vertical structure of wave-averaged cross-shore flow shows a two-dimensional circulation, with onshore flow near surface and an offshore component near the bed. This offshore flow near the bed is also known as undertow, and leads to an offshore directed sediment flux (*Fredsøe and Deigaard*, 1992). How the introduction of the nourishment affects and is affected by these on- and off-shore sediment dynamics is a question that we aim to address here.

Therefore, the goal of this study is to identify the influence of a nourishment on various sediment dynamics and their possible effect on the evolution of the nourishment.

To this end, we develop an idealised model, in which the un-nourished beach is assumed to be in equilibrium. As a first step, we focus on cross-shore process and assume longshore uniform dynamics. Cross-shore sediment flux due to wave skewness, asymmetry, and return flow are considered. The evolution of the nourishment is determined by the perturbation in sediment flux due to the nourishment together with a diffusion term due to down-slope gravity effect, which again acts only on the nourishment (i.e., the deviation from the un-nourished beach).

The model formulation is described in the second section, where wave energy balance, sediment dynamics and nourishment updating are introduced. The model is applied to study the effect and evolution of the nourishment. Model results are presented and analysed in the third section. In section four, the limitations of the model are discussed. Finally, conclusions are given.

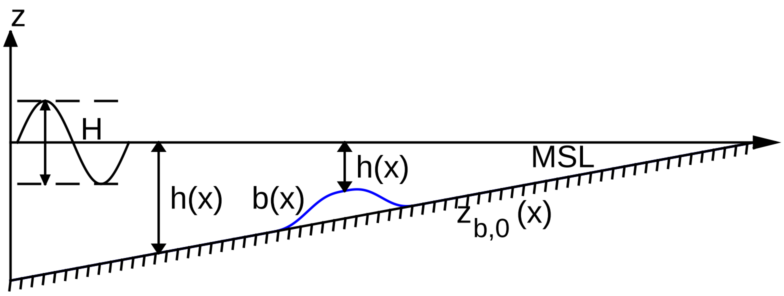

Fig. 1. Geometry and coordinate system.

2 Model Formulation

In this section we develop the evolution equation that describes the nourishment dynamics. To this end we must consider wave height transformation, nonlinear properties associated with the wave, and sediment transport. To begin with, we set out the model geometry.

2.1 Model geometry

A nourishment ($b(x)$) is imposed on a longshore uniform beach (denoted as $z_{b,0}(x)$). x is the cross-shore coordinate, positive onshore. The total water depth is $h(x) = \eta(x) - z_{b,0}(x) - b(x)$. η is the water surface which can shift periodically with tide (see §3.4), otherwise it remains 0. A sketch of the geometry is given in Fig. 1.

2.2 Wave energy balance

Considering a steady, normally incident wave along the offshore boundary, the cross-shore wave energy density ($E_w = \frac{1}{8}\rho g H^2$) transformation follows (*Battjes and Janssen*, 1978)

$$\frac{\partial(E_w c_g)}{\partial x} = -\mathcal{D}_w, \tag{1}$$

where $\rho = 1027\ kg/m^3$ is the water density, $g = 9.81\ m/s^2$ the gravitational acceleration, H the wave height, x the cross-shore coordinate, positive onshore, and c_g is the group velocity resulting from linear wave theory.

Following *van Leeuwen et al.* (2006), the wave energy dissipation ($\mathcal{D}_w$) is parameterized as

$$\mathcal{D}_w = \frac{\rho g \omega B_r^3 H^3}{8\pi h} \left(\frac{H}{\gamma_b h}\right)^m \left(1 - \exp\left(-\left(\frac{H}{\gamma_b h}\right)^n\right)\right). \quad (2)$$

$\omega = \frac{2\pi}{T}$ is the radial frequency of wave of period T, $B_r = 1.0$ is the breaking coefficient, $\gamma_b = 0.6$ the breaker index, and h is the total water depth. Coefficients m and n determine the type of wave. Here we choose $m = 0$ and $n = 20$, which describes a monochromatic wave dissipation based on the bore dissipation model continuously throughout the domain.

To account for the delay in the dissipation process, the roller formulation of *Roelvink and Reniers* (2011) is adopted. The balance of roller energy (E_r) reads

$$\frac{\partial(E_r c)}{\partial x} = \mathcal{D}_w - \mathcal{D}_r, \quad (3)$$

where $c = \frac{\omega}{k}$ is the phase velocity with k being wave number satisfying $\omega^2 = gk \tanh kh$. $\mathcal{D}_r$ is the roller energy dissipation representing the roller energy transfer to turbulent kinetic energy, parameterized as

$$\mathcal{D}_r = 2gE_r \frac{\sin(\beta_r)}{c}, \quad (4)$$

with the slope of the roller/wave front β_r set to 0.1 (*Ruessink et al.*, 2001). The balance of wave and roller energy, i.e., Eq. (1) and (3), are solved using a forward finite difference scheme. On the offshore boundary, a wave of height H_o is imposed, and E_r is set to be 0. The calculation is iterated until convergence in the wave and roller energy are reached. This leads to cross-shore profiles of $H(x)$ and $E_r(x)$ for a given $h(x)$ profile.

2.3 Skewness of wave velocity and acceleration

Using linear wave theory, the cross-shore distribution of wave energy is solved in section 2.2. However, as the wave propagates toward the coast, the wave shape continuously changes from a sinusoidal to a skewed shape in the shoaling region and thereafter to a highly asymmetrical shape after breaking. To account for these wave non-linearities, *Abreu et al.* (2010) proposed a parameterised expression for the near-bed intra-wave orbital velocity:

$$u(t) = u_w \sqrt{1 - r^2} \left\{ \frac{\sin(\omega t) + \frac{r \sin(\phi)}{1+\sqrt{1-r^2}}}{1 - r\cos(\omega t + \phi)} \right\}, \quad (5)$$

with $u_w = \frac{H}{2}\frac{gk}{\omega}\frac{\cosh kz_0}{\cosh kh}$ being the wave orbital velocity at the boundary layer edge z_0 (0.01 m). *Ruessink et al.* (2012) linked parameters r and ϕ to the

Ursell number ($U_r = \frac{3}{8}\frac{kH}{(kh)^3}$), such that

$$r = \frac{2\sqrt{18B^2 + 4B^4}}{9 + 4B^2}, \qquad \phi = -\psi - \frac{\pi}{2}, \tag{6}$$

with B denoting the total non-linearity of the wave, and phase ψ being expressed as

$$B = \frac{p_1}{1 + \exp\left(\frac{p_2 - \log_{10}(U_r)}{p_3}\right)}, \quad \psi = -\frac{\pi}{2} + \frac{\pi}{2}\tanh\left(\frac{p_4}{U_r^{p_5}}\right). \tag{7}$$

$p_1 = 0.79$, $p_2 = -0.61$, $p_3 = 0.297$, $p_4 = 0.64$ and $p_5 = 0.6$ are obtained from *Ruessink et al.* (2012); they result from a least-square fitting with observations. Notice that B and $\psi \to 0$ as $U_r \to 0$; $B \to p_1$ and $\psi \to -\frac{\pi}{2}$ as $U_r \to \infty$.

By definition, the skewness of velocity (S_{vel}) and acceleration (S_{acc}) are written as

$$S_{vel} = \frac{< u^3 >}{\sigma^3(u)}, \quad S_{acc} = \frac{< a^3 >}{\sigma^3(a)}, \tag{8}$$

where $a = \frac{\partial u}{\partial t}$ denotes the local wave acceleration and $< . >$ an average over the wave period. σ refers to the standard deviation of the variable. In this way, S_{vel} and S_{acc} can be calculated with a discretized time series of near-bed intra-wave orbital velocities. This causes a huge calculation burden for the long term evolution, since the discretization, wave averaging and calculation of standard deviation are to be repeated at every node and at every time step. Here, making use of the expression proposed by *Ruessink et al.* (2012), we develop closed form expressions for $\sigma(u)$, $\sigma(a)$, S_{vel} and S_{acc}.

$\sigma(u)$ and $\sigma(a)$ can be approximated as

$$\sigma(u) = u_w(1 - r^2)^{1/2} l(r), \tag{9}$$

$$\sigma(a) = u_w \omega (1 - r^2)^{1/2} f(r), \tag{10}$$

with

$$l(r) = \frac{1}{(1 - r^2)^{1/4}(1 + \sqrt{1 - r^2})^{1/2}} \tag{11}$$

$$f(r) = \sqrt{1/2} + (C_1 - \sqrt{1/2})\frac{l(r) - \sqrt{1/2}}{l(r_\infty) - \sqrt{1/2}} \tag{12}$$

$r_\infty = \lim_{U_r \to \infty} r$. The constant C_1 can be straightforwardly obtained numerically, the method is illustrated in appendix A. S_{vel} and S_{acc} are given as:

$$S_{vel} = B\cos\psi \tag{13}$$

$$S_{acc} = \alpha B \sin(\psi + \pi). \tag{14}$$

α is the ratio $\frac{S_{acc}}{B}$ as $U_r \to \infty$. Detailed derivations are presented in Appendix B.

The expressions in (9), (10), (13) and (14) are used throughout the remainder of the paper for $\sigma(u)$, $\sigma(a)$, S_{vel} and S_{acc} .

2.4 Return flow

Following e.g., *Kuriyama and Nakatsukasa* (2000), we assume that in and out of the surf zone, the return flow (u_{ret}) balances the onshore mass flux driven by wave drift (Q_d), surface roller (Q_r)

$$u_{ret} = -\frac{Q_d + Q_r}{h}, \tag{15}$$

in which

$$Q_d = E_w/(\rho c), \qquad Q_r = 2E_r/(\rho c). \tag{16}$$

2.5 Sediment transport

The wave-skewness-driven near-bed sediment transport follows the form of the *Bailard* (1981) wave-averaged bed sediment flux equation, i.e.,

$$q_{sk} = K_s < u >^3 = K_s S_{vel} \sigma^3(u), \tag{17}$$

where $K_s = 3.5 \times 10^{-4}$ ms^{-2} (from *Bailard* (1981)). The wave-asymmetry-driven bed-load is based on the expression of *Hoefel and Elgar* (2003), i.e.,

$$q_{as} = \begin{cases} K_a(a_{spike} - sign[a_{spike}]a_{crit}) & \text{, if } |a_{spike}| \geq a_{crit} \\ 0 & \text{, if } |a_{spike}| < a_{crit} \end{cases} \tag{18}$$

where $K_a = 2.6 \times 10^{-5}$ ms (*Drake and Calantoni*, 2001), and $a_{spike} = \frac{<a^3>}{<a^2>} = S_{acc}\sigma(a)$. For simplicity, a_{crit} is set to be 0 in this study. The current driven sediment flux is calculated with the formula of Soulsby-VanRijn given by *Soulsby* (1997),

$$q_c = \begin{cases} A_{sb}u_c \left[(u_c^2 + \frac{0.018}{C_D}u_w^2)^{1/2} - u_{cr}\right]^{2.4} & \text{, if } (u_c^2 + \frac{0.018}{C_D}u_w^2)^{1/2} \geq u_{cr} \\ 0 & \text{, if } (u_c^2 + \frac{0.018}{C_D}u_w^2)^{1/2} < u_{cr} \end{cases} \tag{19}$$

For the wave only problem, the current is return flow only, i.e., $u_c = u_{ret}$. q_c is therefore offshore directed. When tide effect is considered, the contribution of tidal current has to be included, as discussed in section 3.4. We neglect the slope effect in the Soulsby-VanRijn formula. $C_D = 0.005$ is the drag coefficient due to current alone. u_{cr} is the threshold current velocity, here we set it as 0 to simplify the problem.

$$A_{sb} = \frac{0.005h(d_{50}/h)^{1.2}}{[(s-1)gd_{50}]^{1.2}}, \tag{20}$$

where $s = 2.65$ is the relative density of sediment, d_{50} is median sediment diameter, see *Soulsby* (1997).

The total sediment transport is therefore the summation of wave skewness, wave asymmetry and return flow driven sediment flux,

$$q = q_{sk} + q_{as} + q_c. \tag{21}$$

Note that we therefore neglect sediment transport due to streaming processes, Stokes drift, and injection of turbulence from breaking (*Roelvink and Reniers*, 2011).

2.6 The evolution equation of nourishment

We assume that a nourishment $b(x)$ is added onto an equilibrium seabed (referred to as $z_{b,0}(x)$). The evolution of the nourishment is subject to

$$\frac{\partial b}{\partial t} + \frac{1}{1-p}\frac{\partial q'}{\partial x} - \gamma\frac{\partial^2 b}{\partial x^2} = 0, \tag{22}$$

where $p = 0.4$ is the porosity of sediment. The perturbed sediment transport q' is given by

$$q' = q(E_w(x), E_r(x), z_{b,0}(x) + b(x)) - q(E_{w,0}(x), E_{r,0}(x), z_{b,0}(x)), \tag{23}$$

and therefore is the cross-shore sediment flux induced by the nourishment. $E_{w,0}$ and $E_{r,0}$ refer to the wave energy density and roller energy on the equilibrium beach ($z_{b,0}$). The third term in (22) represents the diffusion of the nourishment due to gravity. A value of $\gamma = 3.5 \times 10^{-4}$ m^{2}s^{-1} is adopted here as suggested by *Larson and Hanson* (2015).

The divergence of perturbed sediment transport and the diffusion term are calculated using a finite difference scheme. A uniform grid spacing Δx in the cross-shore x axis is considered, with $\Delta x = 1$ m. A so-called Euler-Heun method (*Süli and Mayers*, 2003), i.e., a predictor and corrector algorithm, is applied to update the the shape of the nourishment. In return, the updated nourishment is added to the water depth to calculate the perturbed sediment transport at a new time step. A 0.5 s morphodynamic time step is chosen as a compromise between calculation burden and accuracy. A test with smaller time step showed little difference.

3 Results

The model is first applied to study the evolution of a nourishment deployed on a plane beach in §3.1. The effects of the nourishment on sediment dynamics are then analyzed. Thereafter, we study the effect of nourishment strategy by varying the location of the nourishment while keeping the nourishment volume constant in §3.2. The evolution of the nourishment under various wave conditions (§3.3), i.e., different wave height and period, is also studied. We then consider the effect of the shifting water surface and current due to a tide (§3.4).

3.1 Nourishment deployed on a plane beach

3.1.1 Bathymetry and hydrodynamics

Consider a longshore uniform plane beach, with cross-shore slope of 0.01, see Fig. 1. The offshore boundary is located at $x = 0$, where the water depth is 15 m ($z_{b,0} = -15$ m), the shoreline is at $x = 1500$ m but we terminate the model domain for $h < 0.15$ m. Below this water level, swash zone processes become important which are not accounted for in this model (see *Fernández-Mora et al.*, 2015). A nourishment of the following shape is considered:

$$b(x) = \begin{cases} A_n \left[1 - \frac{|x-x_n|}{L_n} - \frac{\sin(2\pi(1-|x-x_n|/L_n))}{2\pi}\right] & \text{, if } |x - x_n| < L_n, \\ 0 & \text{, otherwise,} \end{cases} \tag{24}$$

where A_n, x_n and L_n are the amplitude, center and half-width of the nourishment. Sand of total amount $A_n L_n$ for every meter is placed. We study here a representative nourishment of 400 m^3/m with $A_n = 2m$, spreading over $700 < x < 1100$ m ($L_n = 200$, $x_n = 900$). The median grain size is $d_{50} = 250$ μm. The size and location of the nourishment and grain size is similar to those implemented along the Dutch coast (*Ojeda et al.*, 2008). The nourishment has a form of a hump on the seabed (see Fig. 1), with minimum total water depth slightly shoreward of x_n, i.e., $x = 950$ m, due to the presence of the background slope.

Wave height (H_o) of 1 m and period (T) of 6 s, is applied at the offshore bound-

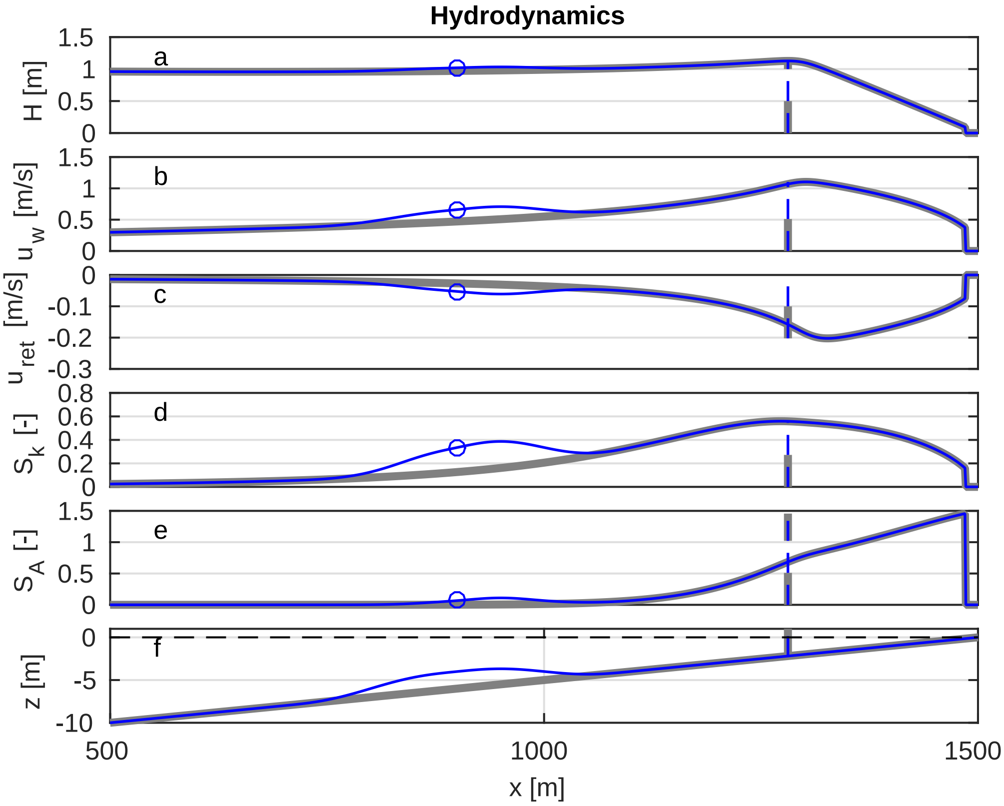

Fig. 2. Cross-shore hydrodynamics: (a), wave height; (b), near bed wave orbital velocity; (c), depth averaged return flow; (d), wave skewness; (e), wave asymmetry, and (f), seabed profile. The thick grey curve refers to the hydrodynamics with original sea bed, the blue curve refers to that with nourished seabed. Blue circle denotes the centre $x_n = 900m$ of the nourishment, and vertical dashed line denotes the breaking location (x_b). Notice that grey and blue dashed lines overlap.

ary. This is to represent a moderately energetic wave condition. In Fig. 2, the cross-shore hydrodynamics with original and nourished seabed is presented.

The wave first shoals, then breaks at around x_b = 1280 m, and gradually decays in the surfzone. The wave orbital velocity follows the distribution of wave height. u_{ret} has its peak further shoreward of the break point. This is due to a phase lag between roller energy (E_r) and wave energy dissipation ($\mathcal{D}_w$) peaks (*Fredsøe and Deigaard*, 1992). The skewness has its peak just prior to breaking. Asymmetry increases monotonically as the shore is approached.

In this example, the introduction of the nourishment does not move the break point. Its effect is to reduce the water depth and thus increase wave height. The near bed wave orbital velocity (u_w) and the return flow (u_{ret}) also increase, as does the wave skewness (S_{vel}). The wave asymmetry (S_{acc}) increases too, but to a lesser extent than S_{vel}.

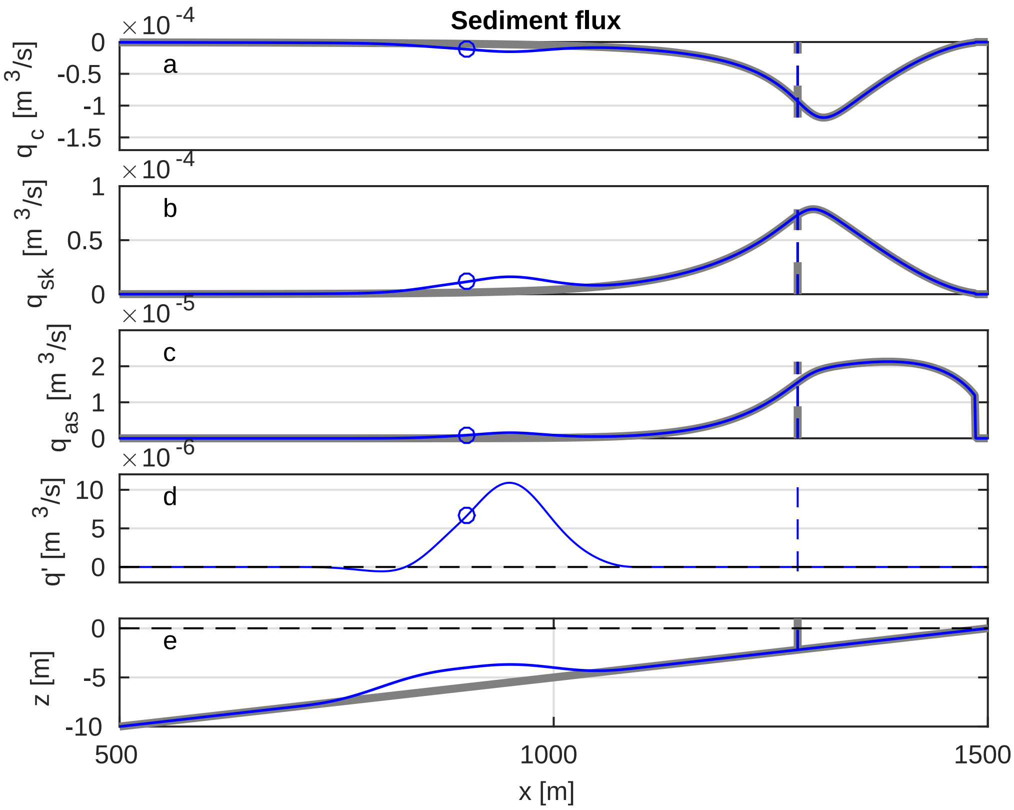

Fig. 3. Sediment flux of: (a), return-flow-driven offshore component q_c; (b), wave skewness driven onshore component q_{sk}; (c), wave asymmetry driven onshore component q_{as}; (d), total perturbed transport q', and (e), seabed profile. Blue circle and vertical dashed line are as in Fig. 2. Similarly, thick grey and thin blue curves represent the case of sea bed without and with nourishment.

3.1.2 Sediment dynamics

Wave skewness and asymmetry drive onshore sediment fluxes (q_{sk} and q_{as}), whereas return flow drives off-shore sediment flux (q_c). The distribution of q_{sk} is a combined effect of S_{vel} and u_w, and so has a peak slightly shoreward of the break point, see Fig 3. q_c has a peak further shoreward of that of q_{sk}, which is due to the delayed peak in u_{ret}. q_{as}, on the other hand, keeps increasing until the post breaking decrease in u_w overwhelms the increase in S_{acc}.

With the implementation of the nourishment, the increase in u_w, u_{ret}, S_{vel} and S_{acc} lead to amplified sediment fluxes, both in the on- and off-shore direction. However, the onshore increase is greater than the equivalent offshore directed sediment flux, resulting in a mostly positive perturbation in the total sediment flux, see Fig 3d. The divergence of a positive q' has positive (negative) value on seaward (shoreward) side of the nourishment (see Fig.4a). This causes erosion on the seaward side of the nourishment and deposition on the shoreward side, and thus leads to an onshore nourishment migration.

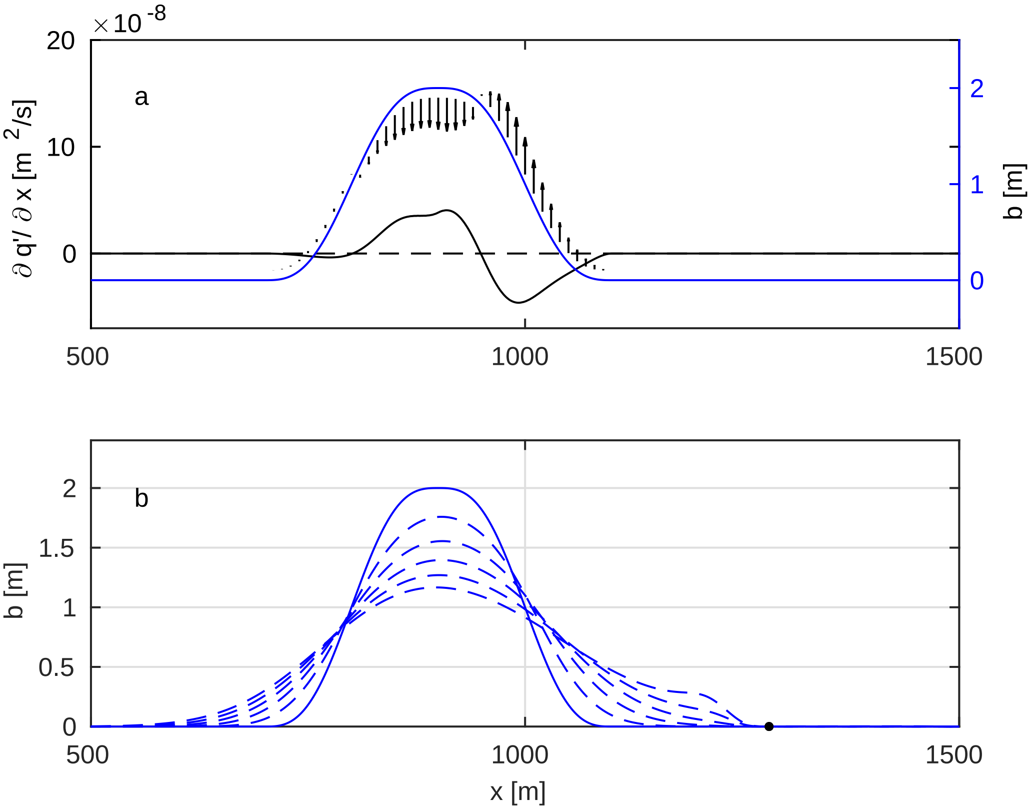

Fig. 4. The evolution of the nourishment for $x_n = 900$ m. a, initial condition for the nourishment: the divergence of q' (black solid line), and the nourishment shape (blue solid line) and movement of the nourishment (indicated by black arrows, upward for deposition and downward for erosion); b, shape of the nourishment at $t = 0$ (blue solid line), and every 30 days after implementation (blue dashed lines), black dots denoting the corresponding location of break point.

3.1.3 Nourishment evolution

Onshore migration of the nourishment is observed (see the hump on the shoreward side of the nourishment in Fig.4b). In the mean time, the diffusion term disperses the nourishment in both on- and off-shore direction. It appears that in this case the diffusion effect is stronger than the divergence of q', since the reduction of the nourishment height is more pronounced than the onshore migration.

The feeder effect of the nourishment located seaward of the breaker zone in moderate wave conditions is in agreement with field observation (*Ojeda et al.*, 2008). Forced by (yearly averaged) H_{rms} of 1 m and $T_s = 6$ s period, the nourishment placed seaward of sandbar (approximately 900 m away from the coast) at Noordwijk (the Netherlands) migrated more than 300 m onshore in 4 years.

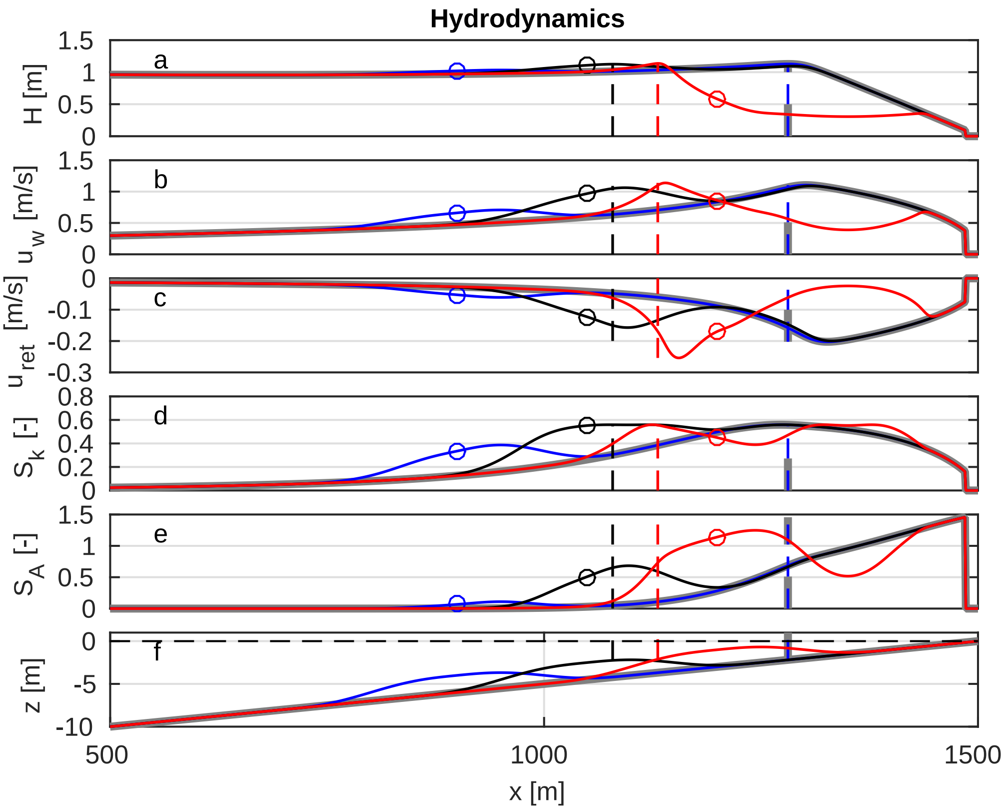

Fig. 5. Cross-shore hydrodynamics and seabed profile for nourishments of $x_n = 900$ m (blue), $x_n = 1050$ m (black) and $x_n = 1200$ m (red). Thick grey (thin) curves represents the case without (with) nourishment. Vertical dashed lines are the location of break points, and circles the location of nourishments.

3.2 Effect of nourishment location

Here, we study the effect of more shoreward nourishment locations by taking $x_n = 1050$ m and $x_n = 1200$ m in (24). The perturbed hydrodynamics are shown in Fig. 5.

The nourishment at $x_n = 1050$ m triggers a first wave break at $x_b = 1079$ m (see vertical black dashed lines in Fig 5). u_w, u_{ret}, S_{vel} and S_{acc} form a peak around this break point. Shoreward of the nourishment, the wave experiences a second shoaling process; as can be seen from Fig. 5, all black curves almost rejoin the thick grey curve at the onshore edge of the nourishment. A second (main) break happens at a location slightly shoreward of the break point of the un-nourished case, with a smaller breaking wave height (H_b). The first wave break is weaker than the second one, as less energy is dissipated (see black curve in Fig. 6).

The perturbed sediment flux (q') for $x_n = 1050$ m has three positive peaks and a negative one (see black curve in Fig. 7d). Seaward of the first break

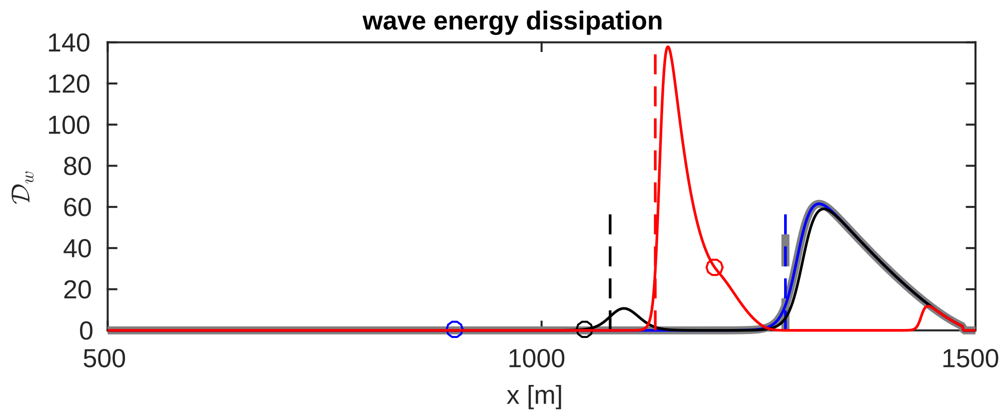

Fig. 6. The distribution of wave energy dissipation $\mathcal{D}_w$ for sea bed with (thin curves) and without nourishment (thick grey), for nourishment placed at $x_n = 900$ m (blue), $x_n = 1050$ m (black) and $x_n = 1200$ m (red). Vertical dashed lines indicate the location of break points.

point, the increase in sediment flux induced by the nourishment is more in the onshore direction than in the offshore, giving a positive q'. q_c predominates during the first wave break, so $q' < 0$ immediately shoreward of the first break point. Further shoreward, the wave stops breaking and shoals, leading to the second positive q'. A third positive q' is shoreward of the nourishment, i.e, $x > 1250$ m, because the effect of a wave energy reduction on q_c is more than that on q_{sk} and q_{as}.

The divergence of q' has a complicated form (see Fig.8a), leading to deposition on top of the nourishment and erosion on both seaward and shoreward sides. Consequently, the nourishment evolves into a skewed shape (see Fig.8c). At the same time, the peak of the nourishment is consistent with the break point and gradually migrates onshore.

The nourishment at $x_n = 1200$ m induces a major break at $x = 1131$ m (see red vertical dashed line in Fig. 5 and Fig. 6). Hydrodynamic quantities achieve local or global maximum around the break point. Compared with the un-nourished case, the majority of wave energy is dissipated further offshore (see red curve in Fig. 6), resulting in the quick drop of H, u_w and u_{ret} after the break.

The profile of q' now has a prominent negative trough and a positive peak further shoreward (see red curve in Fig 7d). The negative perturbation is due to the dominance of q_c in the breaking zone. q' thereafter increases to a peak shoreward of the old break point (grey dashed line). The divergence of q' has a positive value on top of the nourishment and negative value on both seaward and shoreward sides of the nourishment, see Fig. 8b. As a result, a severe erosion is observed on top of the nourishment, which splits the nourishment into two parts, one moving onshore and another offshore (see Fig. 8d).

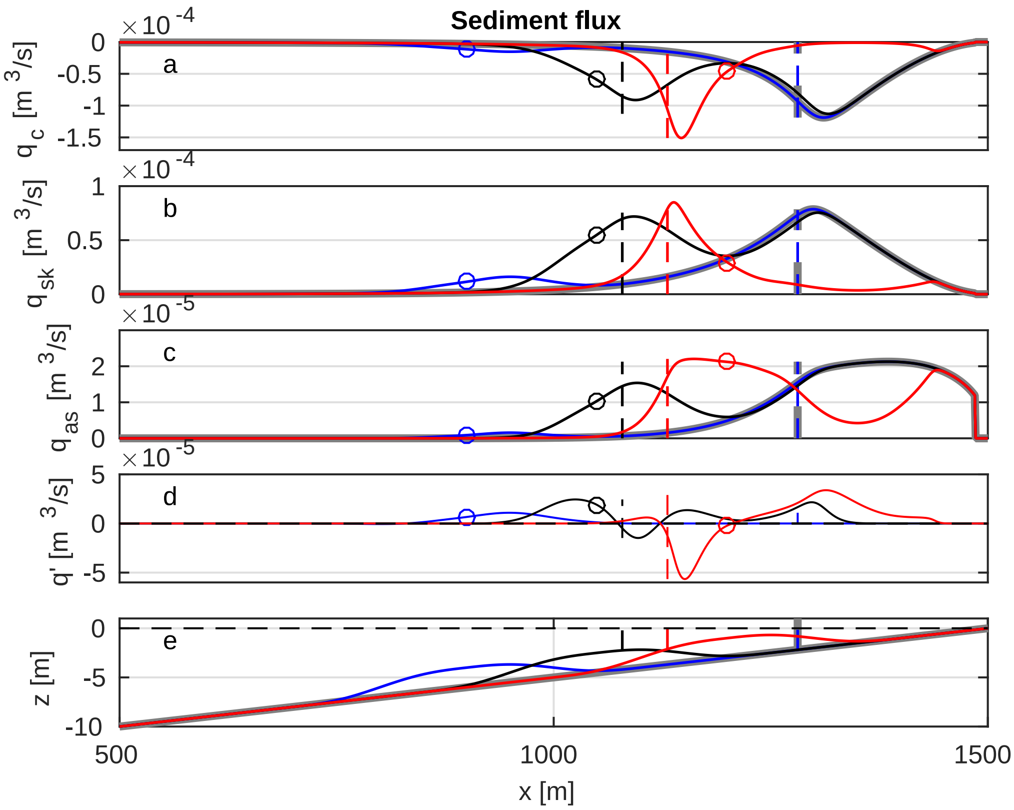

Fig. 7. Sediment fluxes and seabed profile for nourishments of $x_n = 900$ m (blue), $x_n = 1050$ m (black) and $x_n = 1200$ m (red). Thick grey (thin) lines refers to the case without (with) nourishment. Vertical dashed lines describe the location of break point and circles indicate x_n. q' for $x_n = 900$ m and $x_n = 1050$ m (blue and black curve in d panel) are amplified with a factor of 3 for the purpose of better illustration.

The onshore moving nourishment appears to come to rest at the coast and the offshore moving part stabilises with its peak being the new break point. Thereafter, the offshore peak of the nourishment follows the break point and gradually moves onshore, resembling the behaviour of the nourishment placed at $x_n = 1050$ m.

The quick erosion of the nourishment is very close to the evolution of Terschelling (the Netherlands) nourishment (*Grunnet and Ruessink*, 2005). The sand placed in the trough between the middle and the outer bar quickly erodes and forms a new trough within months. Sediment is moved in both directions and incorporated in the middle and outer bar. The markedly different behaviour of $x_n = 1200$ m from $x_n = 1050$ m occurs because of the qualitatively different q' profiles (see Fig. 7d).

As the location of the nourishment moves to the coast, the magnitude and divergence of the q' increases (see Fig 9). As a result, the evolution of the nourishment is much quicker. A nourishment in the offshore causes shoaling and a

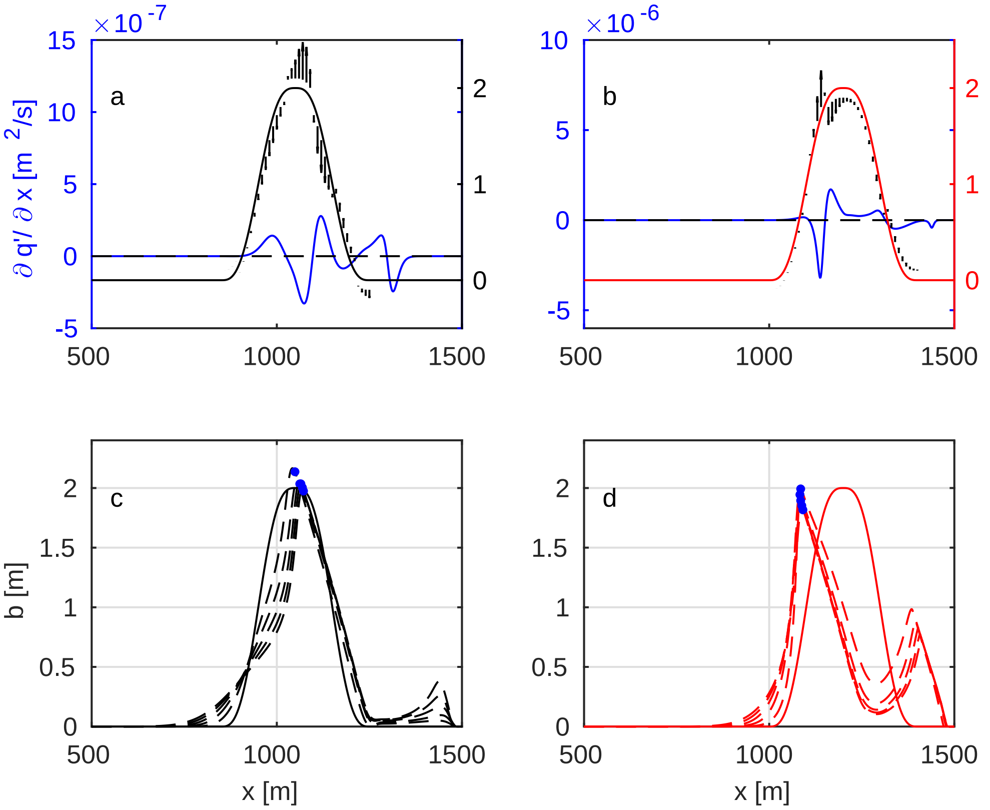

Fig. 8. The evolution of nourishments for $x_n = 1050$ m (a,c) and 1200 m (b,d), under wave of $T = 6$ s, $H_o = 1$ m. a and b, showing the initial condition for nourishments: the divergence of q' (blue curves), nourishment shape (black in a and red in b) and movement (black arrows); c and d, showing the shape of nourishments at every 30 days after implementation (dashed lines in c (black) and d (red)), with blue dots denoting the corresponding break point position.

positive q'. The nourishment will then gradually move to the coast. A nourishment placed close enough to the break point induces an earlier breaking, resulting in a negative q' around the newly formed break point and a positive q' around the break point of the un-nourished beach (see the blue and yellow area in Fig 9). Wave energy is dissipated in this process, the nourishment thus provides a so-called lee effect (*Grunnet et al.*, 2005). The magnitude of q' depends on the intensity of the wave break triggered by the nourishment. The initial evolution of the nourishment then either forms a skewed shape with its peak migrating onshore (weak break) or splits into onshore and offshore parts (strong break).

The original nourishment tends to have a steep (flattened) shape on its seaward (shoreward) side. This is due to the asymmetry in the bed slope. So on the seaward side of the peak of the nourishment, the sea bed has a steeper slope, and the wave shoals and breaks in a shorter distance, with the opposite effect on the shoreward side. Consequently, the magnitude of the divergence of q' is bigger (smaller) on the seaward (shoreward) side of nourishment. The erosion

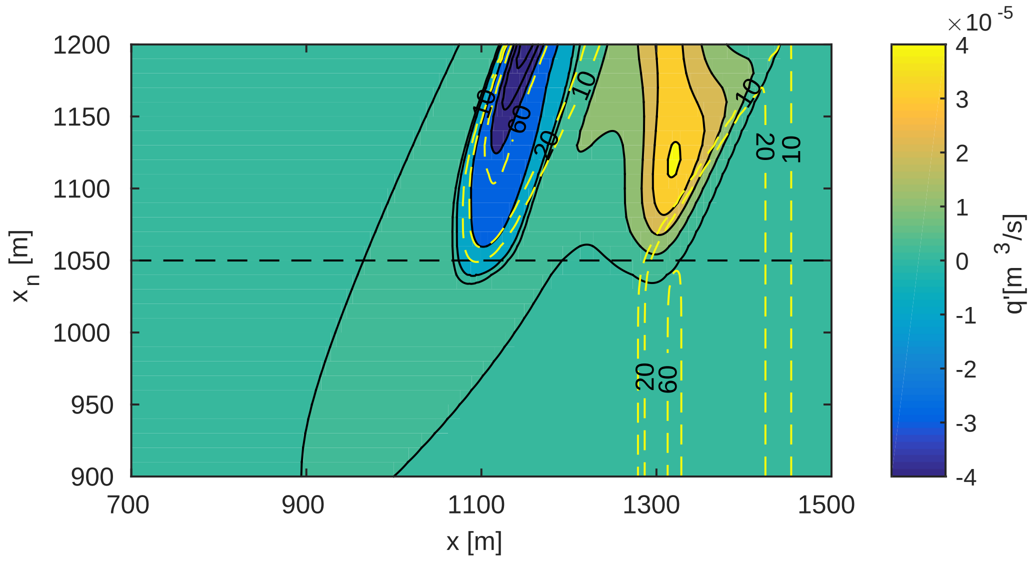

Fig. 9. Sensitivity of the sediment flux perturbation (q') to the location of the nourishment x_n. Color indicates the value of q', with blue for negative and yellow for positive value. Dashed contour lines represents the wave energy dissipation ($\mathcal{D}_w$).

311 on the seaward side is then quicker than the deposition on the shoreward side,
312 which in turn contributes to the asymmetry of the total sea bed slope.

313 *3.3 Sensitivity to wave parameters*

314 *3.3.1 Effect of wave height*

315 To investigate the effect of wave height variation, we consider waves of $H_o =$
316 0.5 m and 2 m (with $T = 6$ s), for $x_n = 900$ m, $A_n = 2$ m and $L_n = 200$
317 m. With increased H_o, H_b increases and x_b moves offshore. Subsequently, the
318 magnitude of u_w and u_{ret} are bigger. S_{vel} and S_{acc} have the same peak value.
319 However, they achieve maximum value further offshore. For higher H_o, the
320 wave shape evolves at a deeper water depth.

321 The magnitude of q_c and q_{sk} significantly increase with increased H_o (see
322 Fig. 10). The maximum magnitude of q_c increases from $4.34\times10^{-5}\ m^3/s$ ($H_o =$
323 0.5 m) to $30 \times 10^{-5}\ m^3/s$ ($H_o = 2$ m). Similarly, the maximum magnitude of
324 q_{sk} increases from $3.31 \times 10^{-5}\ m^3/s$ to $14.9 \times 10^{-5}\ m^3/s$. The nearshore peak
325 of q_{as}, on the other hand, remains fixed. With higher H_o, the increase in q_c
326 is more than the increase in q_{sk}, which results in the domination of offshore
327 directed sediment flux for wave in storm conditions.

328 For all H_o, introduction of the nourishment increases the magnitude of both
329 on- and off-shore directed sediment fluxes. For $H_o = 0.5$ m, the nourishment
330 serves a shoaling effect and induces a positive (onshore) q' (see Fig. 10). The

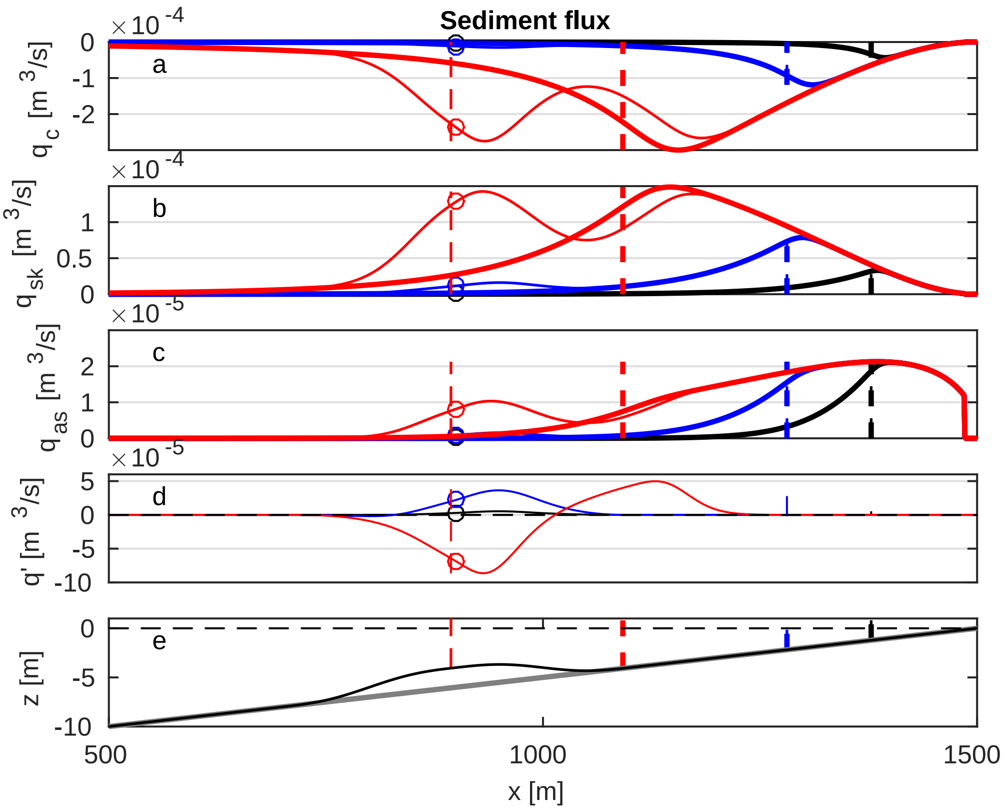

Fig. 10. Sediment dynamics and seabed profile of $H_o = 0.5$ m (black), $H_o = 1$ m (blue) and $H_o = 2$ m (red). Vertical dashed lines indicate the location of break points and circles denoting x_n. The thick and thin lines in each color represent the situation without and with nourishment, respectively. q' for $H_o = 0.5$ m and $H_o = 1$ m (black and blue curve in panel d) are amplified with a factor of 10 for the purpose of better illustration.

divergence of q' thus drives onshore migration of the nourishment, see Fig. 11a. For $H_o = 2$ m, the nourishment induces a wave break at $x_b = 894$ m, leads to a negative (positive) q' around the new (old) break point, see Fig. 10d. The divergence of q' drives offshore nourishment migration, see Fig. 11b. The magnitude of q' increases considerably as H_o increases.

For $H_o = 0.5m$, the diffusion term outweighs the divergence of q'. Therefore, the nourishment disperses in both direction with slightly onshore movement (see Fig.11c). For $H_o = 2$ m, most of the nourishment moves offshore at a much faster speed (see Fig.11d). The transition of onshore migrating nourishment in mild wave conditions to offshore migration in stormy waves is consistent with an earlier study (*Spielmann et al.*, 2011).

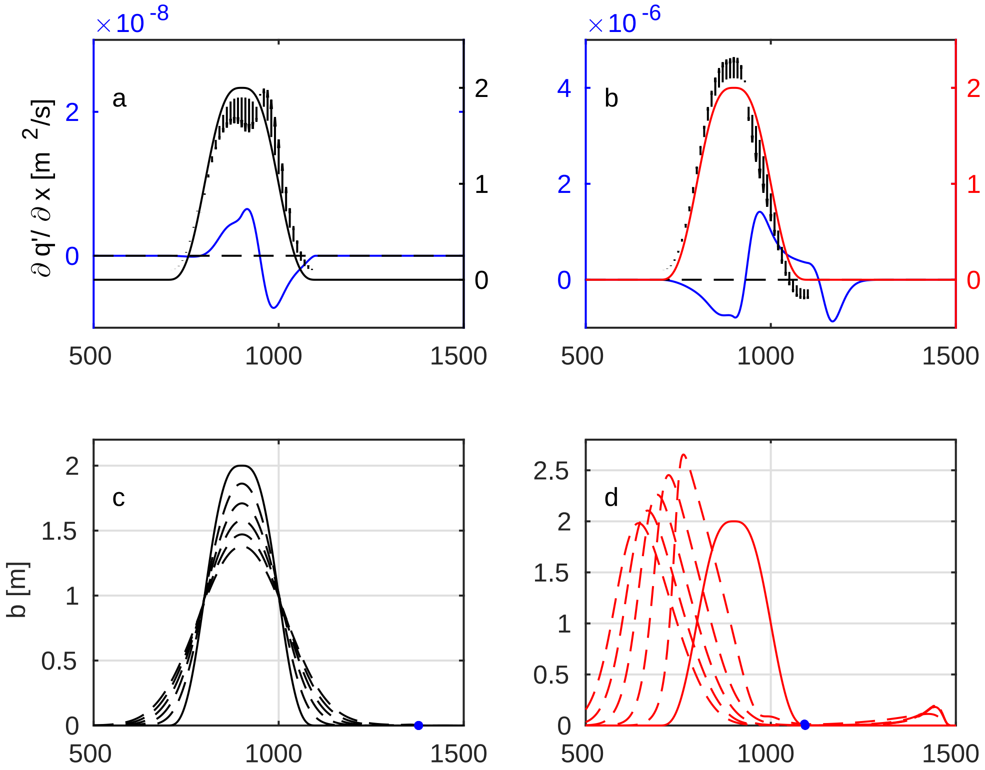

Fig. 11. The evolution of the nourishment for $x_n = 900$ m, under waves of $T = 6$ s, $H_o = 0.5$ m (a,c) and 2 m (b,d). a and b, showing the initial condition for nourishment, the divergence of q' (blue curves), nourishment shape (black curves in a and red in b) and movement (black arrows); c and d, showing the shape of the nourishment at every 30 days after implementation (dashed lines in c (black) and d (red)), with blue dots denoting the corresponding break point position.

3.3.2 Effect of wave period

We consider waves of $T = 3$ s and 10 s (with $H_o = 1$ m), for $x_n = 900$ m, $A_n = 2$ m and $L_n = 200$ m. For $T = 3$ s, H gradually reduces as it propagates to the coast until it breaks at $x_b = 1358$ m. For $T = 10$ s, H keeps growing until it breaks at $x_b = 1238$ m. For larger T, H_b, E_w and E_r increase and so u_{ret} is stronger in the surf zone, and u_w is larger everywhere (also because of smaller kh). Similarly, S_{vel} and S_{acc} reach their maximum value at a deeper water depth. A larger T increases the maximum value of q_c and q_{sk}, but has little influence on that of q_{as}, see Fig. 12. Varying wave period also changes the peak location of sediment dynamics.

For all waves, the nourishment induces a shoaling effect. The effects of nourishment on sediment dynamics are similar for intermediate and long period waves, resulting in a positive q', see Fig. 12. For short wave, in contrast, the increase in q_c due to the presence of the nourishment outcompetes the increase in q_{sk}, therefore leads to a negative q'.

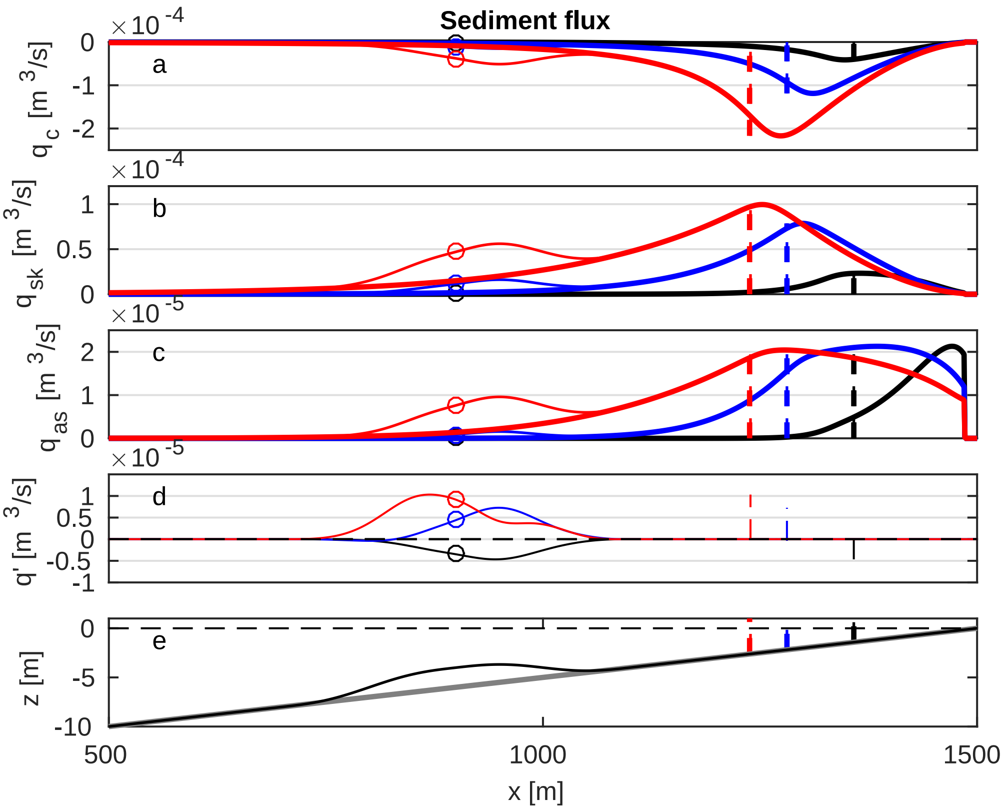

Fig. 12. Sediment fluxes seabed profile for wave of $T = 3$ s (black), $T = 6$ s (blue) and $T = 10$ s (red). Vertical dashed lines indicate the location of break point and circles denoting x_n. The thin and thick lines in each color represent the situation with and without nourishment, with nourishment of $x_n = 900$ m, $L_n = 200$ m and $A_n = 2$ m. H_o for all cases are 1 m. q' for $T = 3$ s and $T = 10$ s (black and blue curve in panel d) are amplified with a factor of 2 for the purpose of better illustration.

This negative q' for $T = 3$ s is due to an overestimation of u_{ret} in the offshore in the expression for Q_d (Eq. (16)). In the model it is implicitly assumed that the onshore flux driven by Stokes drift and wave roller are confined in the upper part of the water column, with return flow in the bottom. Therefore, the current near the bottom is always offshore directed. This is mostly true in the surf zone. However, in the offshore region, the return flow typically happens near the surface (*Lentz et al.*, 2008). Our model thus overestimates u_{ret} in offshore. For $T = 3$ s, use of a more sophisticated model (*Roelvink and Reniers*, 2011) for return flow yields a positive q'.

For $T = 3$ s, diffusion effect remains dominant over the divergence of q'. The nourishment thus spreads in both directions with slightly offshore migration due to the divergence of a negative q' (see Fig.13a and c). For $T = 10s$, the divergence of q' overwhelms the diffusion effect, leading to erosion on seaward of the nourishment and deposition on the peak and shoreward of the nourishment. As a result the nourishment migrates onshore and forms a skewed shape (see Fig.13b and d).

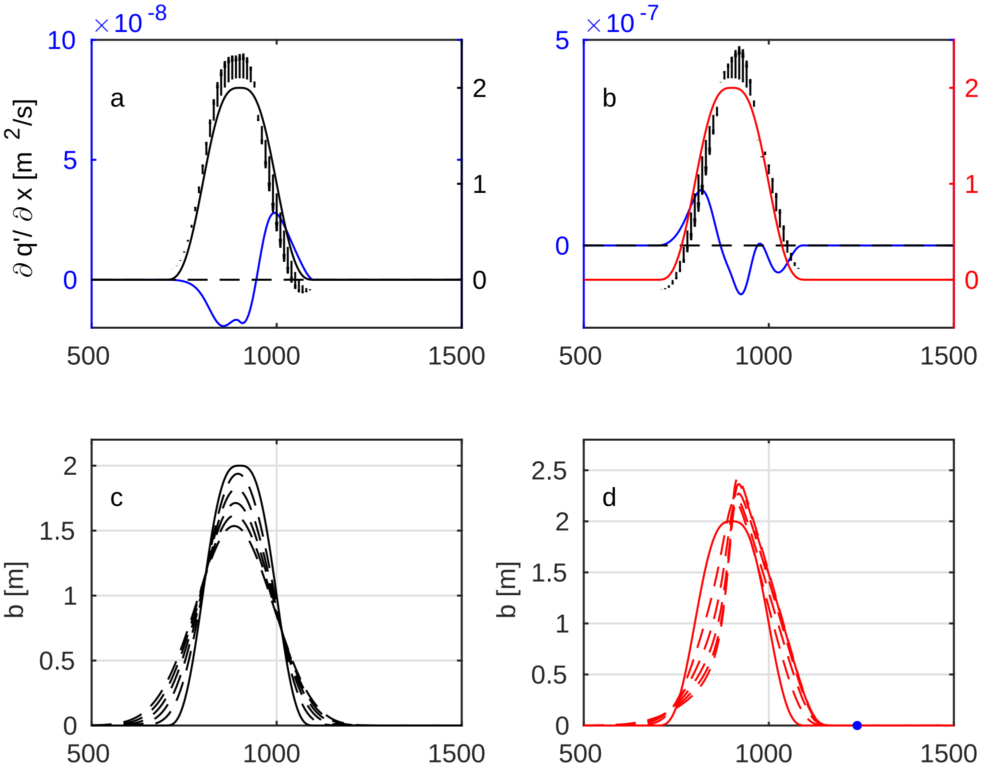

Fig. 13. The evolution of the nourishment for $x_n = 900$ m, under waves of $H_o = 1$ m, $T = 3$ s (a,c) and 10 s (b,d). a and b, showing the initial condition for nourishment, the divergence of q' (blue curves), nourishment shape (black in a and red in b) and movement (black arrows); c and d, showing the shape of the nourishment at every 30 days after implementation (dashed lines in c (black) and d (red)), with blue dots denoting the corresponding break point position.

3.4 Effect of tide

The effect of tide is accounted for by considering the shifting water surface and periodic changing tidal current. An M_2 tide signal with 6 m range is applied. The tidal free surface deviation (η) is assumed to be uniform over the domain. The tidal current (u_T) simply follows the continuity equation (*Schuttelaars and De Swart*, 1999).

$$\eta = A_T \cos(\omega_T t), \tag{25}$$

$$u_T = \frac{\partial \eta}{\partial t}\frac{x_s - x}{h}, \tag{26}$$

with $A_T = 3$ m being tide amplitude, $\omega_T = 2\pi/T_t$ the tidal angular frequency with $T_t = 12h$. x_s refers to the shoreline location, which shifts periodically with tidal level variations. Thus, a nourishment at $x_n = 900$ m, at low tide induces an earlier breaking (see thin red curve Fig.14a), whereas at high tide it just induces a shoaling modification (thin black curve in Fig.14a). The current (u_c) in Eq. (19) is now the combination of tidal current and return

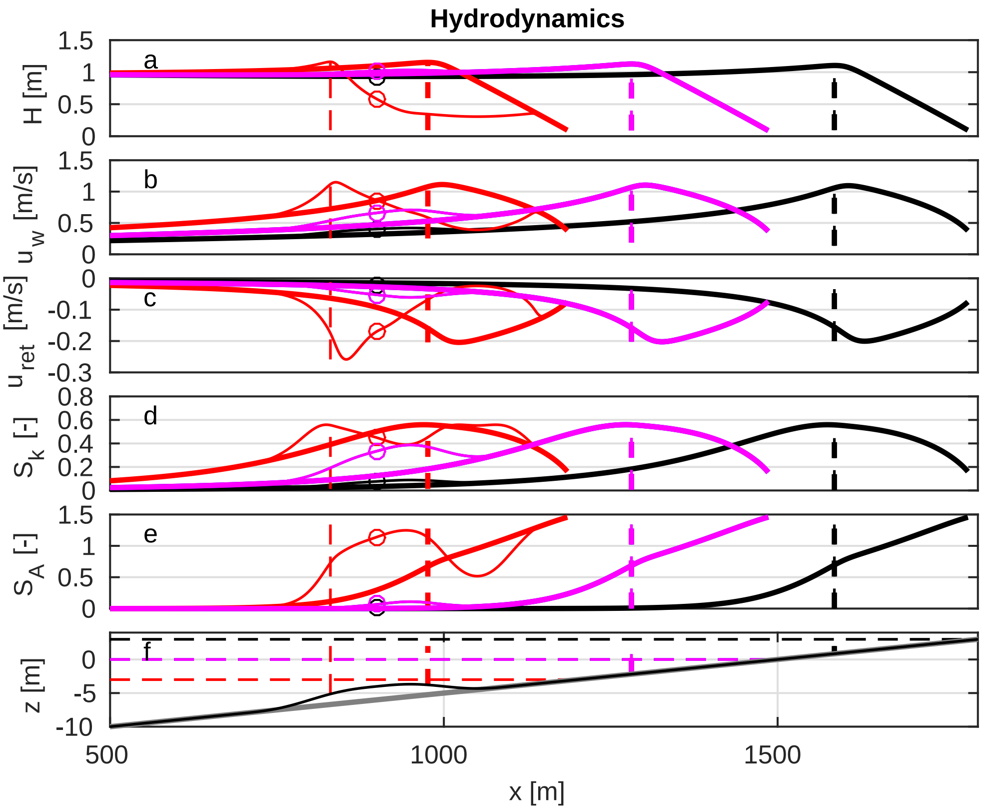

Fig. 14. Hydrodynamics at $t = 0\ T$ (black), $\frac{T}{4}$ (blue), $\frac{T}{2}$ (red) and $\frac{3T}{4}$ (magenta). (f) shows the seabed profile with (thin black) and without (thick grey) nourishment, horizontal dashed lines denoting corresponding tidal level. Vertical dashed lines describe the location of break point and circles indicate x_n. The thin and thick line in each color represents the situation with and without nourishment, with nourishment of $x_n = 900$ m, $L_n = 200$ m and $A_n = 2$ m. The calculation starts from high tide.

flow, i.e., $u_c = u_T + u_{ret}$. Tidal current is maximum at the middle of flood and ebb. On the flood, the onshore directed u_T reduced q_c (magenta curve in Fig.15a), whereas on the ebb, the offshore directed u_T amplifies q_c (blue curve in Fig.15a). Therefore, q' is positive (negative) at $t = \frac{T}{4}$ ($\frac{3T}{4}$), as shown in Fig.15d. The perturbed sediment flux at low tide is the same as the case of $x_n = 1200$ m without tide.

The evolution of the nourishment depends on the the tidally averaged divergence of q'. As shown in Fig.15d, q' at low tide is most significant. The nourishment splits into two parts that migrate in on- and off-shore direction (see Fig.16). The evolution type resembles the case of $x_n = 1200$ m without tide, i.e., Fig.8d, but migrates at a slower rate. The changes on q_c imposed on u_T in flood and ebb tend to compensate for each other. A study was done (not presented) without the tidal current, and results show little difference.

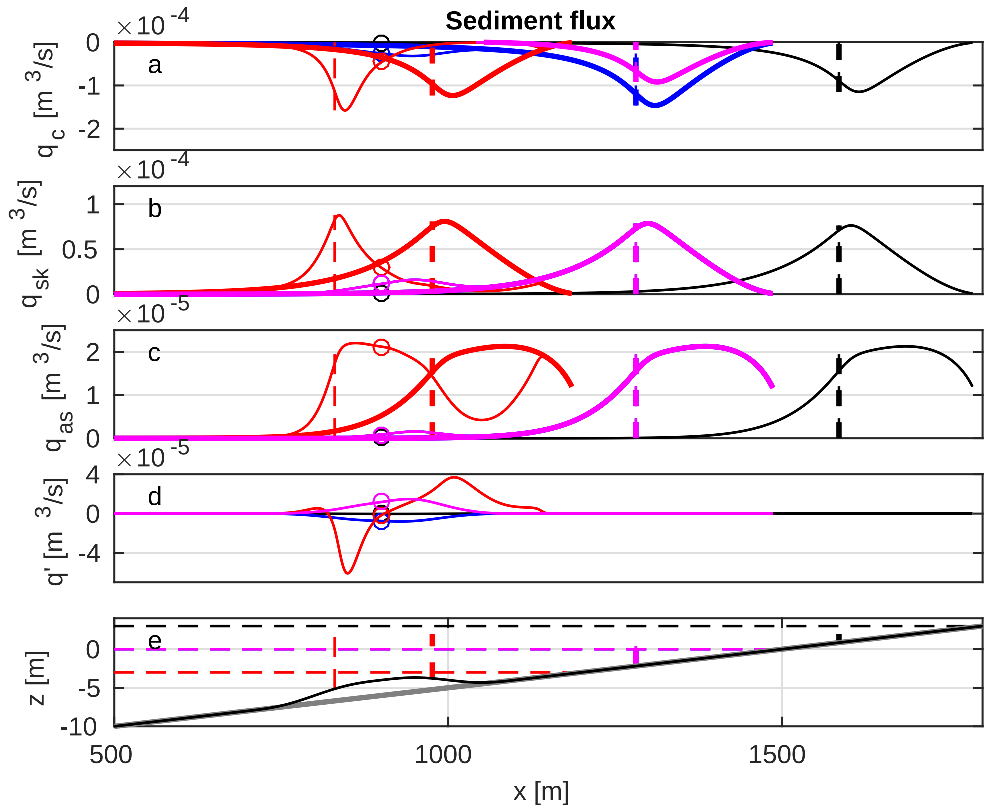

Fig. 15. Sediment dynamics at $t = 0\,T$ (black), $\frac{T}{4}$ (blue), $\frac{T}{2}$ (red) and $\frac{3T}{4}$ (magenta). (e) shows the seabed profile and corresponding tidal level. Vertical dashed lines describe the location of break point and circles indicate x_n. The thin and thick line in each color represents the situation with and without nourishment, with nourishment of $x_n = 900$ m, $L_n = 200$ m and $A_n = 2$ m.

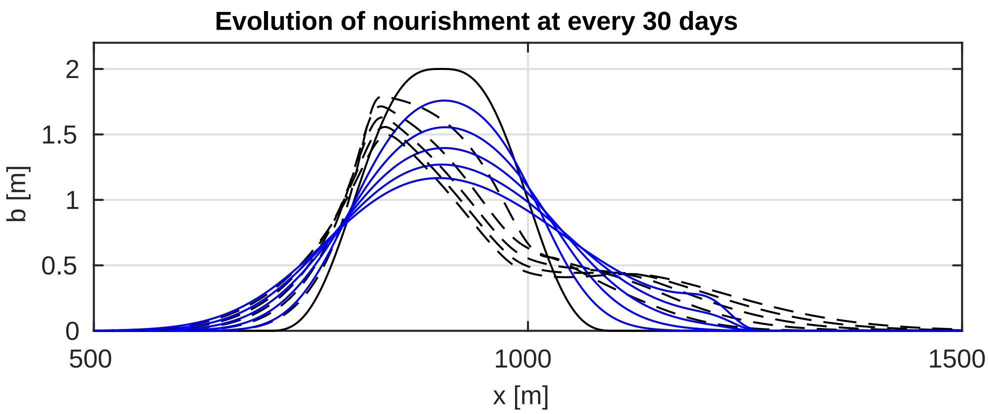

Fig. 16. Nourishment evolution with (black dashed line) and without tide (blue solid lines).

4 Discussion

This model starts with an assumption of an equilibrium beach state, which according to *Dean* (1991) is a profile where all sediment transports are in balance.

Due to the complexity of nearshore sediment dynamics, it takes a long time to obtain an equilibrium beach profile numerically or experimentally. Moreover, with varying wave conditions, such profile can only be approximated by averaging the cross-shore profile over a long period. Since the interest of this paper is in the evolution of the nourishment rather than the coastal profile, we therefore assume that the given beach state is in equilibrium. By doing this, we implicitly assumed a balance between sediment flux driven by wave skewness, wave asymmetry, return flow and gravity driven down slope transport. As such, we interpret the perturbation in down slope transport as the diffusion term in Eq. (22). Studies (not shown here) with different beach profiles, i.e., plane beaches with different slope and beaches with nearshore sand bar, show that the physics examined in this paper pertains to other initial beach profiles. Despite its simplicity, an equilibrium beach assumption is useful for interpreting the coastal engineering process (*Dean*, 2003).

In this model we considered dominant processes in the complex nearshore sediment dynamics, i.e., the wave skewness and asymmetry-driven onshore sediment flux, the return flow driven offshore sediment flux, and the gravity driven diffusion effect. As mentioned in §2.4, Stokes drift drives a net onshore water mass. The associated sediment flux is thought to be small compared with other mechanisms, for the Stokes drift exists in the upper part where the sediment concentration is relatively small. Streaming-driven sediment flux is also neglected due to its weak magnitude (*Roelvink and Reniers*, 2011). Suspended-load is not included in this model. This is because in many wave-averaged formulas suspended-load is found to be roughly proportional to bed-load (*Fernández-Mora et al.*, 2015). Thus, inclusion of suspended-load makes no qualitative difference to the balance of sediment fluxes considered here.

For a nourishment project, a primary concern is the direction of migration of the nourishment, which depends on the divergence of q'. Theoretically, the divergence of q' can be written as $\frac{\partial q'}{\partial x} = \frac{\partial q'}{\partial b}\frac{\partial b}{\partial x} + \frac{\partial q'}{\partial E'_w}\frac{\partial E'_w}{\partial x} + \frac{\partial q'}{\partial E'_r}\frac{\partial E'_r}{\partial x}$, with b the bed perturbation, and E'_w and E'_r denoting the perturbation in wave and roller energy.

We can thus rewrite Eq. (22) (excluding diffusion) as:

$$\frac{\partial b}{\partial t} + \frac{1}{1-p}\frac{\partial q'}{\partial b}\frac{\partial b}{\partial x} = -\frac{1}{1-p}\left\{\frac{\partial q'}{\partial E'_w}\frac{\partial E'_w}{\partial x} + \frac{\partial q'}{\partial E'_r}\frac{\partial E'_r}{\partial x}\right\}, \tag{27}$$

where it can be seen that $c_n = \frac{1}{1-p}\frac{\partial q'}{\partial b}$ represents its intrinsic propagation speed, whereas $\frac{\partial q'}{\partial E'_w}$ and $\frac{\partial q'}{\partial E'_r}$ are part of a forcing term. Assuming a bed perturbation, i.e., nourishment, of small amplitude (ϵ), which induces a corresponding small change in total water depth but a negligible change in wave and roller energy, i.e., $E'_w \approx E'_r \approx 0$, then the nourishment is subject only to migration at its intrinsic propagation speed c_n. Expanding q' in a Taylor ex-

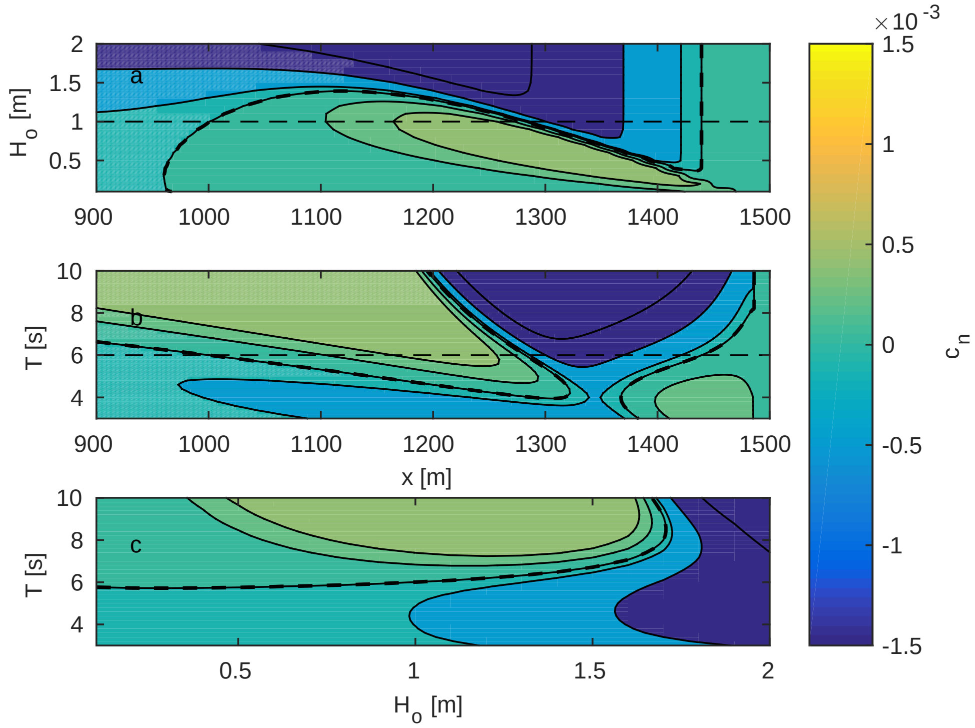

Fig. 17. Sensitivity of c_n to: a, H_o (from 0.1 to 2 m), with $T = 6$ s; b, T (from 3 to 10 s), with $H_o = 1$ m; c, H_o (from 0.1 to 2 m) and T (from 3 to 10 s), evaluated at $x = 1000$ m. Zero contour lines are highlighted as thick dashed lines.

pansion of ϵ, $q' = \frac{\partial q}{\partial b}|_{b=0}\epsilon + \mathcal{O}(\epsilon^2)$, c_n is then approximated based on dynamics of the basic state. Here we take the linear term. We can then examine c_n as a function of x for varying T and H_o; see Fig.17a and b.

For $H_o = 1$ m and $T = 6$ s (see horizontal dashed lines in Fig.17a and b), c_n changes from positive (onshore migrating) in the shoaling zone to negative (offshore migrating) shoreward of the break point. c_n is again negative offshore for smaller periods (see Fig.17 b), but this is due to breakdown of the approximation of u_{ret} in that region (see §3.3.2). Note that the onshore propagation of the nourishment for $x_n = 900$ m and $A_n = 2$ m (in §3.1) is not captured in Fig.17a and b. This is in part because of the aforementioned u_{ret} approximation, and also because the small nourishment yields a larger water depth compared with that for the $A_n = 2$ m nourishment.

Consistent with our model results, c_n is mostly positive for mild and moderate wave, and negative for stormy wave, see Fig.17a. For waves of longer period, the magnitude of c_n is larger (see Fig.17b). Meanwhile, the change from positive to negative c_n is shifted offshore for long period waves due to relatively shallower water further offshore.

For a nourishment at a particular location, this method provides a straightforward way to illustrate the possible migration direction (see Fig.17c, for

$x = 1000$ m).

The analysis applied here only considers the linear term and neglects the change in E_w and E_r, but it gives a reasonable first approximation of the migrating direction of the nourishment, particularly in the shoaling zone. In the surf zone, we may expect the forcing term in Eq. (27) to be prominent, and so this approximation analysis will be less appropriate.

For simplicity, our model neglects the threshold of motion of sediment, which leads to an overestimation of sediment flux. However, the qualitative behavior of sediment dynamics remains the same. The effect of nourishment and its evolution will therefore be qualitatively the same with the inclusion of a threshold.

In this study, we adopt an idealised method in order to isolate physics and for rapid numerical solution. In principle the approach we use could be undertaken with a complex numerical model.

5 Conclusion

In this paper, we have developed an idealised model to study the cross-shore evolution of a nourishment. Wave and roller energy balance are solved to obtain wave height, near bed wave orbital velocity and return flow. Following *Ruessink et al.* (2012), the wave nonlinearity is parameterized using a formula based on the Ursell number. New expressions for skewness and standard deviation of wave velocity and acceleration are introduced. The new expressions greatly accelerate the calculation. Sediment flux driven by wave skewness, asymmetry (both onshore) and return flow (offshore) are calculated. The implementation of the nourishment perturbs the wave and sediment dynamics previously assumed to be in equilibrium. The evolution of the nourishment thus is subject to the divergence of total sediment flux perturbation (q'), and a diffusion term simulating downslope movement of the bed sediment due to gravity.

The divergence of a positive (negative) q' results in onshore (offshore) migration of the nourishment. For waves in stormy weather, the return-flow-driven sediment flux dominates the sediment dynamics. In these circumstances, the nourishment tends to induce a negative q' and migrates offshore, which is consistent with earlier observations.

In the shoaling zone, under moderate and mild waves, onshore sediment fluxes outcompete the offshore flux. The nourishment in general migrates onshore, but its evolution is sensitive to the relative location of the nourishment and wave break point. Deployed at a location well away from the break point (seaward), the nourishment induces a shoaling effect and amplifies all sediment processes. Due to the dominance of onshore directed sediment transport in this region, the nourishment causes a positive q'. The nourishment diffuses and slowly moves onshore, therefore provides a 'feeder' effect. Positioned close enough to the break point, the nourishment induces an earlier breaking, dissipates wave energy and provides a so-called 'lee' effect. Around the new break point, $q' < 0$ due to the predominance of return flow driven sediment flux. The energy being dissipated in this process results in a diminution in all sediment processes shoreward of the nourishment. However, the return flow driven offshore flux is particularly reduced and leads to a positive q'. Depending on the intensity of the earlier breaking, the nourishment either moves onshore or splits into two parts. For a weak break, the nourishment formed a skewed shape and its peak follows the break point and gradually migrates onshore. For a strong break, i.e., when most of the wave energy is been dissipated, severe erosion is observed on the peak of the nourishment. The nourishment then splits into two parts, one moving onshore and another offshore. The offshore moved nourishment stops as its peak coincide with the wave break point, and thereafter, gradually migrates onshore.

The effects of a longer wave period on the nourishment are twofold. Firstly, the magnitude of q' increases with T, resulting in a quicker evolution of the nourishment. Secondly, the active zone of wave dynamics is shifted offshore for longer period wave, which changes the relative location of the nourishment and break point, thus changing the evolution type of the nourishment. Furthermore, tide affects nourishment evolution through shifting the relative location of the nourishment and break point as the water surface changes periodically. Tidal elevation is shown to be more important than tidal current. The q' at low tide determines the evolution of the nourishment.

We also studied the intrinsic propagation speed of the nourishment which shows that it can be used as a first approximation of the migrating direction of the nourishment.

Our model neglects a few processes including the sediment flux due to Stokes drift and streaming and the threshold of sediment initiation. At present, the model only considers a shoreface nourishment. To study the evolution of a beach nourishment, a wetting and drying scheme must be included. The model is limited to cross-shore evolution of the nourishment, whereas in reality, further complexity arises from two dimensional dynamics. A next step would be to extend this model to two horizontal dimensions.

Acknowledgements

The support of the UK Engineering and Physical Sciences Research Council (EPSRC) under the MORPHINE project (grant EP/N007379/1) and of the University of Nottingham is gratefully acknowledged.

References

Abreu, T., P. A. Silva, F. Sancho, and A. Temperville, Analytical approximate wave form for asymmetric waves, *Coast. Eng.*, *57*(7), 656 – 667, doi: 10.1016/j.coastaleng.2010.02.005, 2010.

Bailard, J. A., An energetics total load sediment transport model for a plane sloping beach, *J. Geophys. Res. : Oceans*, *86*(C11), 10,938–10,954, doi: 10.1029/jc086ic11p10938, 1981.

Battjes, J. A., and J. P. F. M. Janssen, *Energy Loss and Set-Up Due to Breaking of Random Waves*, chap. 32, pp. 569–587, doi: 10.1061/9780872621909.034, 1978.

Capobianco, M., H. Hanson, M. Larson, H. Steetzel, M. J. F. Stive, Y. Chatelus, S. Aarninkhof, and T. Karambas, Nourishment design and evaluation: applicability of model concepts, *Coast. Eng.*, *47*(2), 113 – 135, doi:10.1016/s0378-3839(02)00123-0, 2002.

Dean, R. G., Equilibrium beach profiles: characteristics and application, *J. Coast. Res.*, *7*(1), 53–84, 1991.

Dean, R. G., *Beach Nourishment*, world scientific, doi:10.1142/2160, 2003.

Drake, T. G., and J. Calantoni, Discrete particle model for sheet flow sediment transport in the nearshore, *J. Geophys. Res. : Oceans*, *106*(C9), 19,859–19,868, doi:10.1029/2000JC000611, 2001.

Fernández-Mora, A., D. Calvete, A. Falqués, and H. E. de Swart, Onshore sandbar migration in the surf zone: New insights into the wave-induced sediment transport mechanisms, *Geophys. Res. Let.*, *42*(8), 2869–2877, doi: 10.1002/2014GL063004, 2015.

Fredsøe, J., and R. Deigaard, *Mechanics of Coastal Sediment Transport*, world scientific, doi:10.1142/1546, 1992.

Grunnet, N. M., and B. Ruessink, Morphodynamic response of nearshore bars to a shoreface nourishment, *Coast. Eng.*, *52*(2), 119 – 137, doi: 10.1016/j.coastaleng.2004.09.006, 2005.

Grunnet, N. M., B. G. Ruessink, and D. R. Walstra, The influence of tides, wind and waves on the redistribution of nourished sediment at Terschelling, The Netherlands, *Coast. Eng.*, *52*(7), 617 – 631, doi: 10.1016/j.coastaleng.2005.04.001, 2005.

Hamm, L., M. Capobianco, H. H. Dette, A. Lechuga, R. Spanhoff, and M. J. F.

Stive, A summary of european experience with shore nourishment, *Coast. Eng.*, *47*(2), 237 – 264, doi:10.1016/S0378-3839(02)00127-8, 2002.

Henderson, S. M., J. S. Allen, and P. A. Newberger, Nearshore sandbar migration predicted by an eddy-diffusive boundary layer model, *J. Geophys. Res. : Oceans*, *109*(C6), doi:10.1029/2003JC002137, 2004.

Hoefel, F., and S. Elgar, Wave-induced sediment transport and sandbar migration, *Science*, *299*(5614), 1885–1887, doi:10.1126/science.1081448, 2003.

Kuriyama, Y., and T. Nakatsukasa, A one-dimensional model for undertow and longshore current on a barred beach, *Coast. Eng.*, *40*(1), 39 – 58, doi: 10.1016/S0378-3839(00)00005-3, 2000.

Larson, M., and H. Hanson, Model of the evolution of mounds placed in the nearshore, *Journal of Integrated coastal zone management*, *15*(1), 21 – 33, doi:10.5894/rgci530, 2015.

Lentz, S. J., M. Fewings, P. Howd, J. Fredericks, and K. Hathaway, Observations and a model of undertow over the inner continental shelf, *J. of Phys. Oceanogr.*, *38*(11), 2341–2357, doi:10.1175/2008JPO3986.1, 2008.

Ojeda, E., B. G. Ruessink, and J. Guillen, Morphodynamic response of a two-barred beach to a shoreface nourishment, *Coast. Eng.*, *55*(12), 1185 – 1196, doi:10.1016/j.coastaleng.2008.05.006, 2008.

Roelvink, D., and A. Reniers, *A Guide to Modeling Coastal Morphology*, WORLD SCIENTIFIC, doi:10.1142/7712, 2011.

Ruessink, B. G., J. R. Miles, F. Feddersen, R. T. Guza, and S. Elgar, Modeling the alongshore current on barred beaches, *J. Geophys. Res. : Oceans*, *106*(C10), 22,451–22,463, doi:10.1029/2000JC000766, 2001.

Ruessink, B. G., G. Ramaekers, and L. C. van Rijn, On the parameterization of the free-stream non-linear wave orbital motion in nearshore morphodynamic models, *Coast. Eng.*, *65*, 56 – 63, doi:10.1016/j.coastaleng.2012.03.006, 2012.

Samaras, A. G., M. G. Gaeta, A. M. Miquel, and R. Archetti, High-resolution wave and hydrodynamics modelling in coastal areas: operational applications for coastal planning, decision support and assessment, *Nat. Hazards and Earth Sys.*, *16*(6), 1499–1518, doi:10.5194/nhess-16-1499-2016, 2016.

Schuttelaars, H. M., and H. E. De Swart, Initial formation of channels and shoals in a short tidal embayment, *J. Fluid Mech.*, *386*, 1542, doi: 10.1017/S0022112099004395, 1999.

Soulsby, R., *Dynamics of marine sands, a manual for practical applications*, 249 pp., Thomas Telford, 1997.

Spielmann, K., R. Certain, D. Astruc, and j P Barusseau, Analysis of submerged bar nourishment strategies in a wave-dominated environment using a 2dv process-based model, *Coast. Eng.*, *58*, 767–778, doi: 10.1016/j.coastaleng.2011.03.015, 2011.

Süli, E., and D. F. Mayers, *An Introduction to Numerical Analysis*, Cambridge University Press, doi:10.1017/CBO9780511801181, 2003.

van Duin, M. J. P., N. R. Wiersma, D. J. R. Walstra, L. C. van Rijn, and M. J. F. Stive, Nourishing the shoreface: observations and hindcasting of the Egmond case, The Netherlands, *Coast. Eng.*, *51*(8), 813 – 837, doi:

10.1016/j.coastaleng.2004.07.011, coastal Morphodynamic Modeling, 2004.

van Leeuwen, S. M., N. Dodd, D. Calvete, and A. Falqués, Physics of nearshore bed pattern formation under regular or random waves, *J. Geophys. Res. : Earth Surface*, *111*(F1), doi:10.1029/2005JF000360, 2006.

van Leeuwen, S. M., N. Dodd, D. Calvete, and A. Falqués, Linear evolution of a shoreface nourishment, *Coast. Eng.*, *54*(5), 417 – 431, doi: 10.1016/j.coastaleng.2006.11.006, 2007.

van Veelen, T., P. Roos, and S. Hulscher, Process-based modelling of bank-breaking mechanisms of tidal sandbanks, *Cont. Shelf Res.*, *167*, 139–152, doi:10.1016/j.csr.2018.04.007, 2018.

A Standard deviation of u and a

By definition, $\sigma(u)$ is written as

$$\sigma(u) = \sqrt{\frac{1}{N-1}\sum_{i=1}^{N}(u_i - < u >)^2}, \tag{A.1}$$

where u_i denotes the discretized intra-wave velocity. Assuming that the water particle follows a closed orbital trajectory, so $< u >= 0$, then $\sigma(u)$ is

$$\sigma(u) = \sqrt{< u^2 >} = U_w\sqrt{1-r^2}\sqrt{\frac{1}{T}\int_0^T\left(\frac{\sin(\omega t) + r\sin(\phi)/(1+\sqrt{1-r^2})}{1 - r\cos(\omega t + \phi)}\right)^2 dt}. \tag{A.2}$$

Now let $\tilde{u} = \frac{\sin(\theta)+r\sin(\phi)/(1+\sqrt{1-r^2})}{1-r\cos(\theta+\phi)}$ with $\theta = \omega t$, $\sigma(u)$ is then

$$\sigma(u) = U_w\sqrt{1-r^2}\sqrt{\frac{1}{2\pi}\int_0^{2\pi}\tilde{u}^2 d\theta}. \tag{A.3}$$

The integration $\sqrt{\frac{1}{2\pi}\int_0^{2\pi}\tilde{u}^2 d\theta}$ is solved analytically, and is found to be only dependent on r. Therefore,

$$\frac{\sigma(u)}{U_w\sqrt{1-r^2}} = l(r) = \frac{(1-r^2)^{-1/4}}{(1+\sqrt{1-r^2})^{1/2}}. \tag{A.4}$$

Similarly, the standard deviation of acceleration $\sigma(a)$ is

$$\sigma(a) = \sqrt{< a^2 >} = \omega U_w\sqrt{1-r^2}\sqrt{\frac{1}{2\pi}\int_0^{2\pi}\tilde{a}^2 d\theta}, \tag{A.5}$$

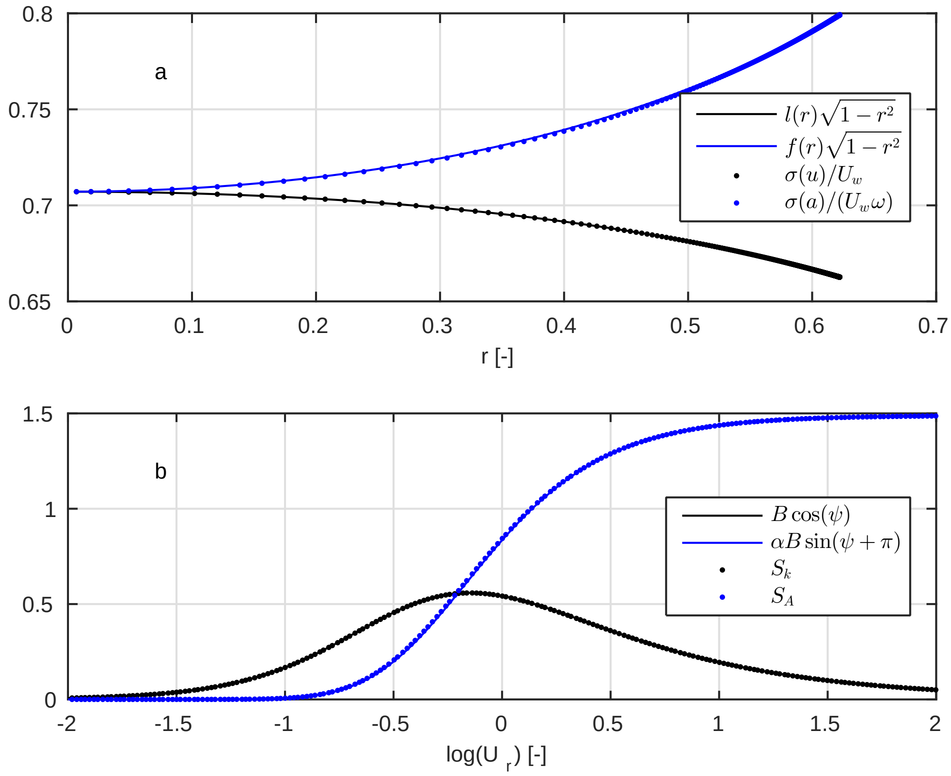

Fig. A.1. a, comparison of $\sigma(u)$ (black) and $\sigma(a)$ (blue) calculated by definition (dots) and expressions (A.4), (A.6) (solid curves). b, comparison of S_{vel} (black) and S_{acc} (blue) calculated by definition (dots) and equation (B.2), (B.3) (solid curves).

with $\tilde{a} = \frac{\cos(\theta)-r\cos(\phi)-r^2\sin(\phi)\sin(\theta+\phi)/(1+\sqrt{1-r^2})}{(1-r\cos(\theta+\phi))^2}$. The integration of $\sqrt{\frac{1}{2\pi}\int_0^{2\pi}\tilde{a}^2 d\theta}$ is found to be dependent on r and can be approximated as

$$\frac{\sigma(a)}{\omega U_w\sqrt{1-r^2}} \approx f(r) = \sqrt{1/2} + (C_1 - \sqrt{1/2})\frac{l(r)-\sqrt{1/2}}{l(r_\infty)-\sqrt{1/2}} \tag{A.6}$$

where C_1 is the value of the $\sqrt{\frac{1}{2\pi}\int_0^{2\pi}\tilde{a}^2 d\theta}$ as $U_r \to \infty$, and is numerically obtained by evaluating $\sqrt{\frac{1}{2\pi}\int_0^{2\pi}\tilde{a}^2 d\theta}$ with $U_r = 600$. A comparison of $\sigma(u)$ and $\sigma(a)$ calculated by definition (i.e., (A.1)) and our expressions (A.4, A.6) is given in Fig. A.1a.

B Skewness of wave velocity S_{vel} and acceleration S_{acc}

With the expression of $\tilde{u}$ and $\tilde{a}$, the skewness of wave velocity and acceleration can be written as,

$$S_{vel} = \sqrt{2\pi}\frac{\int_0^{2\pi} \tilde{u}^3 d\theta}{\sqrt{\int_0^{2\pi} \tilde{u}^2 d\theta}^3}, \quad S_{acc} = \sqrt{2\pi}\frac{\int_0^{2\pi} \tilde{a}^3 d\theta}{\sqrt{\int_0^{2\pi} \tilde{a}^2 d\theta}^3}. \tag{B.1}$$

Exact expression of S_{vel} and S_{acc} are relying on the expression of the integrations, which are very complicate. Luckily, early study by *Ruessink et al.* (2012) can be used to achieve simple forms for S_{vel} and S_{acc}. In *Ruessink et al.* (2012), the skewness of wave velocity (denoted as S_u) and hilbert transformation of wave velocity (denoted as A_u) were combined into the total non-linearity B and phase ψ, implying that $S_u = B\cos(\psi)$ and $A_u = B\sin(\psi)$. Therefore, the skewness of velocity is simply

$$S_{vel} = B\cos(\psi). \tag{B.2}$$

We found that the skewness of acceleration (S_{acc}) follows the same shape as A_u but with a phase shift and a multiplication factor.

$$S_{acc} = \alpha B \sin(\psi + \pi), \tag{B.3}$$

ideally, α is the limit of $\frac{S_{acc}}{B}$ as $U_r \to \infty$. Here, the value of α is numerically obtained by evaluating $\frac{S_{acc}}{B}$ with $U_r = 600$, where S_{acc} is calculated using equation (B.1). A comparison of S_{vel} and S_{acc} calculated by definition (i.e., Eq. (8)) and our expressions (A.4) and (A.6) is given in Fig. A.1b.

Highlight

- An idealised one dimensional (cross-shore) morphodynamic model that couples wave, tide and sediment dynamics is developed to study the effect and evolution of a shoreface nourishment.
- In moderate and mild wave conditions, a nourishment placed well offshore from the break point induces an overall positive perturbation in sediment flux, resulting in onshore migration (feeder effect). Located closer to the break point, the nourishment induces an earlier wave breaking, which dissipates part of the wave energy (lee effect), resulting in onshore migration (weak break) or splitting into onshore and offshore moving parts (strong break). In storm wave conditions, nourishment moves offshore due to the predominance of return-flow-driven sediment flux.
- Tide affects nourishment evolution through shifting the relative location of the nourishment and break point. The sediment dynamics at low tide dominate the evolution of the nourishment.